Systems & Control Transactions

Original Research Article
Peer Reviewed Conference Proceeding
ESCAPE 36 - European Symposium on Computer Aided Process Engineering
Sheffield, UK. 21-24 June 2026

PSE PRESS

Managing Renewable Energy Uncertainty in Green Hydrogen Production Systems

Matteo Lea Casagrande, Andrea Isella, and Davide Manca*

PSE-Lab, Process Systems Engineering Laboratory, Dipartimento di Chimica, Materiali e Ingegneria Chimica "Giulio Natta", Politecnico di Milano, Piazza Leonardo da Vinci 32, 20133 Milano, Italy
* Corresponding Author: davide.manca@polimi.it.

ABSTRACT

The extensive use of renewable energy to supply hydrogen production for chemical processes is hindered by the uncertainty in power generation and by strict operational limits.These challenges are addressed through a real-time dynamic optimization approach based on a receding-horizon strategy that provides optimal decision variables. The framework explicitly relies on imperfect weather forecasts and dynamically adapts the hydrogen reference production to guarantee the final productivity target. The optimization methodology focuses on minimizing grid electricity imports, limiting excessive equipment stress, and preventing constraint violations, while ensuring that the hydrogen production target is satisfied.The proposed approach yields competitive economic and environmental performance, with a levelized cost of hydrogen of 3.31 USD/kg$_{H_2}$, well within literature values (1.50–7.50 USD/kg$_{H_2}$) and below typical industrial costs (4–12 USD/kg$_{H_2}$). At the same time, carbon dioxide emissions are reduced by more than 90% compared to steam methane reforming, resulting in specific emissions below 1 kg$_{CO_2}$/kg$_{H_2}$. These results are supported by a year-long simulation based on CAISO renewable energy data. The optimized system achieves the annual hydrogen production target while respecting all operational constraints, whereas the absence of operational strategy and buffering systems leads to systematic constraint violations. The strategy can be implemented in existing industrial facilities with limited modifications.

Keywords: Green hydrogen, Real-time dynamic optimization, Forecast uncertainty, Receding horizon, Power-to-Hydrogen

INTRODUCTION

Global scenario

The urgency surrounding industrial decarbonization has intensified as CO_2 emissions from human activities continue to increase. Recent data from 2024 indicate that emissions from energy generation, fuel combustion, and manufacturing operations have reached 37.6 Gt$_{CO_2}$ annually, an 8.4% increase relative to levels observed ten years earlier [1]. Direct emissions from industrial sources (Scope 1) represent approximately 23% of this global total, not accounting for the substantial indirect emissions associated with energy consumption across these operations.

Among industrial sectors, chemical manufacturing presents particularly high carbon intensity. Traditional synthesis pathways for several foundational chemicals result in considerable emission factors: ammonia production generates up to 4.6 kg$_{CO_2}$/kg$_{NH_3}$, methanol up to 2.8 kg$_{CO_2}$/kg$_{CH_3OH}$, nitric acid up to 1.6 kg$_{CO_2}$/kg$_{HNO_3}$, and hydrogen up to 26 kg$_{CO_2}$/kg$_{H_2}$. When accounting for both on-site emissions and those associated with purchased energy, the chemical industry is responsible for approximately 6.4% of global greenhouse gas releases [2].

Concurrently, the renewable energy sector has undergone substantial expansion. European markets illustrate this transition: the share of renewables in total energy consumption increased from 9.6% in 2004 to 24.5% by 2023 [3]. While this growth trajectory presents opportunities for reducing carbon emissions in chemical production, it simultaneously introduces operational challenges due to the intermittent nature of wind and solar power generation.

Renewable energy sources

Solar photovoltaic and onshore wind technologies exhibit favorable characteristics for industrial deployment due to their modularity and minimal site-specific requirements. Nevertheless, the temporal variability inherent to these sources necessitates effective energy conversion and storage infrastructure to ensure process continuity.

For renewable-powered hydrogen generation, proton exchange membrane (PEM) electrolysis systems demonstrate superior performance under dynamic operating conditions compared to alkaline technologies, despite the latter's higher technology readiness level and lower capital expenditure. Regarding energy storage architectures, battery energy storage systems (BESS) deliver high round-trip efficiencies and rapid power response characteristics, while compressed hydrogen storage represents the most established and cost-effective approach for hydrogen inventory management.

Plant design and operation in literature

Existing literature on renewable-hydrogen system design predominantly emphasizes techno-economic optimization under steady-state or quasi-static operating assumptions [4, 5]. Reported levelized costs for hydrogen production typically range from 3 to 4 USD/kg$_{H_2}$, with regional variations driven by resource availability: lower values observed in high-resource regions and elevated costs documented across European installations [6]. The operational performance of these systems under transient renewable supply conditions remains insufficiently characterized.

Current research on operational control strategies frequently relies on deterministic renewable energy forecasts or omits critical process-side constraints [7, 8]. As a result, methodologies capable of addressing renewable variability, equipment operational limits, downstream process requirements, and economic objectives within a unified framework remain underdeveloped.

This study presents a real-time, multi-objective optimization framework for integrated renewable-hydrogen production systems operating under uncertainty. The framework incorporates forecast error propagation, dynamic control variable adjustment, degradation-aware operation, and hydrogen demand satisfaction constraints. The methodology enables techno-economically optimized operation under realistic industrial conditions and is directly applicable to commercial-scale green hydrogen facilities with minimal adaptation requirements.

METHODOLOGY

System description

The integrated system for hydrogen production comprises renewable power generation units (wind and solar photovoltaic) coupled with a PEM water electrolysis unit. To attenuate high-frequency power fluctuations, lithium-ion BESS and compressed hydrogen storage vessels are implemented as buffering components. The system interfaces with both the electrical grid and the downstream hydrogen-consuming process.

As illustrated in **Figure 1**, power from the renewable generation and grid connection is distributed between the BESS and the electrolyzer. Hydrogen produced by the electrolyzer is partitioned between the storage vessels and the downstream facility. During periods of insufficient renewable generation, electrical energy and hydrogen are supplied from BESS discharge and tank depletion, respectively.

The system dynamics can be expressed mathematically as follows:

$$E_{ren} + E_{grid} = E_{bess} + E_{el} \tag{1}$$

$$F_{el} = c_{el} \cdot E_{el} \tag{2}$$

$$F_{el} = F_{tank} + F_{plant} \tag{3}$$

$$\frac{dQ_{bess}}{dt} = \eta_{bess} \cdot E_{bess} - \kappa_{bess} \cdot Q_{bess} \tag{4}$$

$$\frac{dm_{tank}}{dt} = \eta_{tank} \cdot F_{tank} - \kappa_{tank} \cdot m_{tank} \tag{5}$$

Each variable corresponds to the mass and energy streams depicted in **Figure 1**. The parameter c_{el} represents the electrolyzer conversion coefficient for hydrogen production, while η and κ denote the charging efficiency and self-discharge rate for the BESS and hydrogen storage.

Since E_{ren} is determined by exogenous renewable resource availability, the system contains 8 variables. Given 5 governing equations, the formulation exhibits 3 degrees of freedom.

Approach to the problem

Given weather forecast data over the next $t_{regulation}$ time steps, the system has $3 \cdot t_{regulation}$ degrees of freedom. Following a receding horizon strategy, the optimal decision variable trajectory is computed via optimization, with only the initial time step implemented and subsequent values discarded upon re-optimization [9].

This formulation shares conceptual similarities with model predictive control (MPC) frameworks [10]. However, whereas MPC constitutes an advanced real-time control architecture, the proposed methodology generates optimal reference production trajectories for implementation within existing control systems. In other words, the proposed methodology constitutes a supervisory optimization layer that provides optimal setpoints corresponding to the optimal configuration of the decision variables, while real-time tracking and disturbance rejection are handled by the underlying control system. The design and implementation of such control systems

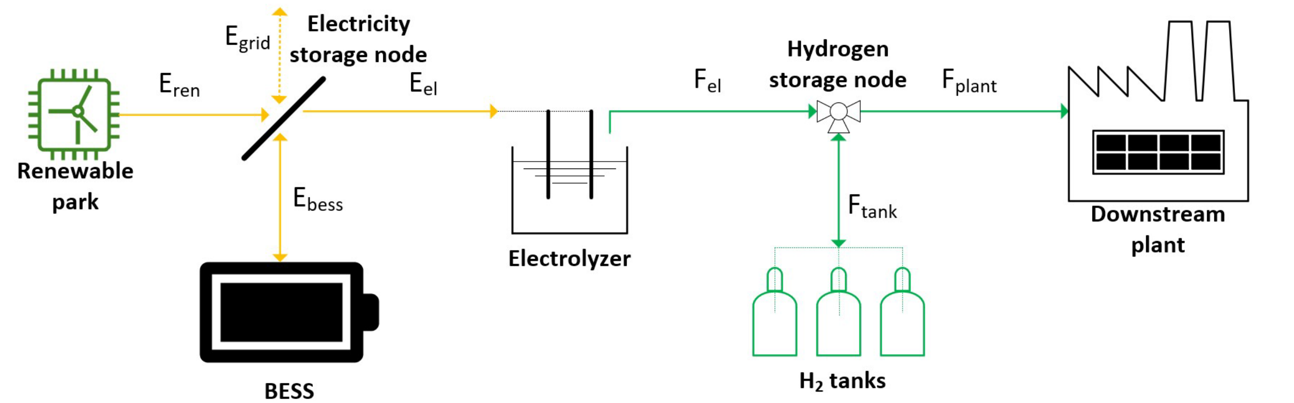

Figure 1. Hydrogen production plant scheme.

are beyond the scope of this work, as the focus is on the optimization-based determination of the setpoint.

The optimization requires specification of the three manipulated variables per time step, selected as E_{bess}, F_{tank}, and E_{grid} based on their direct controllability. The primary objective ensures that F_{plant} tracks the specified hydrogen demand profile for each time step.

$$f_{rp} = \sum_{t=1}^{t_{regulation}} k_1 \cdot \left| \frac{F_{plant}^t - F_{plant}^{rp}}{F_{plant}^{rp}} \right| \tag{6}$$

Additionally, to minimize equipment degradation, solutions exhibiting reduced high-frequency variability are favored. This applies specifically to hydrogen flow to the downstream process, electrical power to the electrolyzer, and charging/discharging rates of the buffer systems.

$$f_{var} = \sum_{t=1}^{t_{regulation}} \left(k_2 \cdot \left| \frac{F_{plant}^t - F_{plant}^{t-1}}{F_{plant}^{rp}} \right| + k_3 \cdot \left| \frac{E_{bess}^t - E_{bess}^{t-1}}{Q_{bess}^{max}} \right| + k_4 \cdot \left| \frac{F_{tank}^t - F_{tank}^{t-1}}{m_{tank}^{max}} \right| + k_5 \cdot \left| \frac{E_{el}^t - E_{el}^{t-1}}{E_{el}^{nominal}} \right| \right) \tag{7}$$

The economic impact of grid interaction must also be incorporated, accounting for electricity import costs and export revenues (which may be positive, negative, or zero depending on market conditions).

$$f_{grid} = \sum_{t=1}^{t_{regulation}} \left(k_6 \cdot \max\left(E_{grid}^t, 0\right) + k_7 \cdot \min\left(E_{grid}, 0\right) \right) \tag{8}$$

Operational constraints are imposed to ensure solution feasibility. Two constraint categories are defined: bounds on state and control variables to enforce operational limits and physical constraints, and rate-of-change limitations to restrict ramping behavior. Each penalty term equals the constraint violation magnitude multiplied by an appropriate penalty coefficient, or zero when the constraint is satisfied.

$$P_{value}: \begin{cases} Q_{bess}^{min} \le Q_{bess}^t \le Q_{bess}^{max} \\ m_{tank}^{min} \le m_{tank}^t \le m_{tank}^{max} \\ E_{el}^{min} \le E_{el}^t \le E_{el}^{max} \\ F_{plant}^{min} \le F_{plant}^t \le F_{plant}^{max} \end{cases} \tag{9}$$

$$P_{var}: \begin{cases} \left|E_{bess}^t - E_{bess}^{t-1}\right| \le \delta_{bess}^{max} \\ \left|F_{tank}^t - F_{tank}^{t-1}\right| \le \delta_{tank}^{max} \\ \left|E_{el}^t - E_{el}^{t-1}\right| \le \delta_{el}^{max} \\ \left|F_{plant}^t - F_{plant}^{t-1}\right| \le \delta_{plant}^{max} \end{cases} \tag{10}$$

The complete objective function is formulated as:

$$\Phi = f_{rp} + f_{var} + f_{grid} + P_{value} + P_{var} \tag{11}$$

Minimization of the objective function

Minimization of the objective function presents computational challenges due to its inherent non-convexity and potentially large dimensionality. Furthermore, variations in the weighting coefficients (k_1 to k_7) can result in objective function values spanning several orders of magnitude.

The scaling issue is addressed through a double-logarithmic transformation of the objective function, with an offset term to prevent numerical singularities:

$$\hat{\Phi} = \log_{10}(\log_{10}(\Phi + 10)) \tag{12}$$

The non-convexity is handled by exploiting the cusp-like topology of the objective function, as identified through preliminary grid-search analysis. Under these conditions, Powell's conjugate direction method demonstrates robust convergence behavior. Alternatively, genetic algorithms can be employed to guarantee global optimality, albeit with higher computational expense.

The high-dimensional search space is handled through a warm-start initialization strategy [11], wherein the discarded portion of the previous optimization solution provides the initial guess for subsequent iterations:

$$X_{first\ guess}^{\theta+1} = [X_2^{\theta}, X_3^{\theta}, X_4^{\theta}, \dots, X_{t_{regulation}-1}^{\theta}, X_{t_{regulation}}^{\theta}, X_{t_{regulation}}^{\theta}] \tag{13}$$

where X represents an arbitrary decision variable stream. The final time step is replicated since $t_{regulation}$ initial values are required while only $t_{regulation}-1$ values are available from the previous solution. For the initial simulation step, where no prior solution exists, genetic algorithms are employed due to their lack of initialization requirements.

Renewable energy forecast modeling

Given the reliance on imperfect renewable energy forecasts and the difficulty in obtaining extended-horizon predictions at high temporal resolution, synthetically generated forecast data are employed in this analysis.

Artificial forecasts are derived from historical renewable generation profiles through application of two sequential perturbations: Savitzky-Golay filtering and time-dependent stochastic deviation.

The Savitzky-Golay filter attenuates high-frequency components while preserving underlying trends, thereby replicating the smoothing effect inherent to forecast models with limited temporal resolution.

Time-dependent stochastic perturbations are subsequently applied to represent forecast degradation with increasing prediction horizon. The filtered profile is modulated by a scaling factor incorporating both temporal distance from the present and normally distributed random variability:

$$\varepsilon_{eff} = (u_1 + u_2 \cdot t) \cdot rand_{normal} \tag{14}$$

$$E_{ren}^{forecast} = E_{ren}^{SG-filtered} \cdot (1 + \varepsilon_{eff}) \tag{15}$$

where the parameters u_1 and u_2 characterize forecast accuracy, and $E_{ren}^{SG-filtered}$ denotes the Savitzky-Golay-filtered generation profile.

This methodology enables a realistic representation of operational forecast behavior, yielding results consistent with actual forecasting system performance.

Constraint-correction procedure

Due to discrepancies between optimal solution computed using forecast data and actual system behavior under real renewable generation profiles, constraint violations may occur during implementation despite satisfying constraints during optimization.

To address this issue, a post-processing correction procedure is applied at each time step to enforce constraint satisfaction based on realized operating conditions.

The correction algorithm proceeds hierarchically from downstream process requirements toward upstream renewable generation. For each system variable (flows and inventories), feasibility is evaluated against operational bounds. When violations are detected, the manipulated variables are adjusted to restore constraint satisfaction.

For a generic variable X, the corrected value X^{final} and the constraint function ψ_j to be satisfied are defined as:

$$X^{final} = \begin{cases} X^{max} & if\ X > X^{max} \\ X & if\ X^{min} \le X \le X^{max} \\ X^{min} & if\ X < X^{min} \end{cases} \tag{16}$$

$$\psi_j = model^X(E_{bess}, F_{tank}, E_{grid}) - X^{final} \tag{17}$$

Where $model^X$ represents the governing equation for variable X.

The hierarchical structure processes constraints sequentially. Initially, the constraint function ψ for F_{plant} is enforced through adjustment of F_{tank}. Subsequently, two independent subsystems address constraints on m_{tank} and E_{el}, coupled respectively with F_{plant} through F_{tank} and E_{bess} adjustments.

Finally, to satisfy the BESS charge constraint Q_{bess}, the corresponding function ψ is incorporated into a system coupling F_{plant} and E_{el} constraints, with all three manipulated variables available for adjustment.

During resolution of the E_{el} system, the previously corrected m_{tank} value may not be preserved; however, this does not compromise system feasibility to all operational bounds. Physically, when energy surplus causes tank saturation, excess power is redirected to the BESS rather than the electrolyzer. In the limiting case where electrolyzer power remains above maximum capacity, power reduction yields a tank inventory slightly below maximum but always exceeding the uncorrected optimization result. Analogous reasoning applies to renewable energy deficit conditions, ensuring no operational conflicts arise.

Productivity target enforcement

The methodology enforces production of a target hydrogen quantity over the simulation period:

$$M_{H_2}^{total} = F_{plant}^{nominal} \cdot \theta_{tot} \tag{18}$$

where $F_{plant}^{nominal}$ denotes the downstream facility nominal flow rate and θ_{tot} represents the total simulation duration.

To achieve this cumulative production target, the F_{plant} reference production requires dynamic adjustment at each time step to account for deviations from nominal production. The objective is precise attainment of $M_{H_2}^{total}$

rather than production maximization.

The cumulative hydrogen production up to time θ can be expressed in discrete form as:

$$M_{H_2}(\theta) = M_{H_2}^{\theta} = \sum_{i=0}^{\theta} F_{plant}^{i} \bullet \Delta\theta \quad (19)$$

To satisfy the productivity constraint, the updated reference production $F_{plant}^{rp\ new}$ must compensate for the remaining production requirement:

$$M_{H_2}^{\theta} + F_{plant}^{rp\ new} \bullet (\theta_{tot} - \theta) = F_{plant}^{nominal} \bullet \theta_{tot} \quad (20)$$

Yielding:

$$F_{plant}^{rp\ new} = \frac{F_{plant}^{nominal} \bullet \theta_{tot} - M_{H_2}^{\theta}}{\theta_{tot} - \theta} \quad (21)$$

The updated reference production is subsequently bounded within operational limits F_{plant}^{min} and F_{plant}^{max}.

This formulation exhibits fundamental limitations: when the computed reference production saturates at either bound, the productivity target becomes unattainable, as the physically required reference production exceeds the admissible operating range. Additionally, stochastic fluctuations cause the average production to systematically deviate from the reference production when operating at the constraints, progressively amplifying the deviation between ideal and constrained reference production values.

An alternative formulation addresses this issue by distributing the production deficit over a fraction of the remaining horizon rather than the entire duration. The original formulation is designated the "ideal reference production, " representing the constant flow rate that would achieve the target productivity. The modified formulation, with α denoting the fraction of remaining time considered, becomes:

$$F_{plant}^{rp\ new} = F_{plant}^{nominal} + \frac{F_{plant}^{nominal} \bullet \theta - M_{H_2}^{\theta}}{(\theta_{tot} - \theta) \bullet \alpha} \quad (22)$$

This expression is also subject to feasibility constraints within operational bounds.

The revised formulation allows the ideal reference production to converge toward nominal conditions, thereby reducing cumulative productivity deviations.

Both formulations exhibit pronounced oscillatory behavior near simulation termination, as illustrated in **Figure 2**, attributable to the diminishing remaining time in the denominator, which amplifies the sensitivity to production deviations.

Figure 2 also demonstrates that reference productions persistently exceed nominal production rates throughout most of the simulation period. This phenomenon arises because renewable energy deficits necessitate elevated reference productions, while surplus renewable generation is preferentially allocated to buffer charging rather than production intensification.

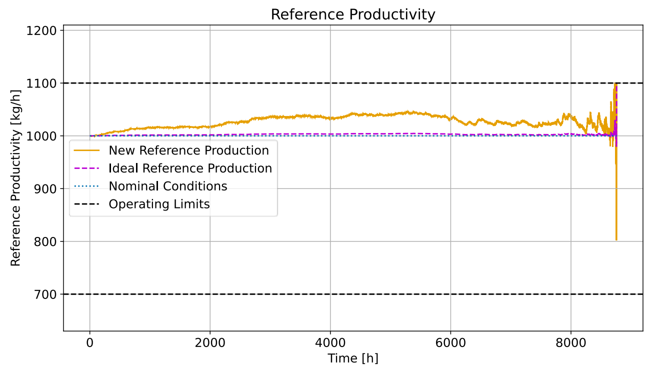

Figure 2: Comparison of the reference productions: "new" (solid orange), "ideal" (dashed magenta) and nominal conditions (dotted blue).

RESULTS AND DISCUSSION

The proposed methodology is validated through a case study focused on hydrogen production for a downstream ammonia plant. Renewable energy availability is derived from data provided by the California Independent System Operator (CAISO) [12] from 2020.

The optimal sizing of the units, the definition of nominal operating conditions for the downstream plant, and the identification of operational constraints are determined using the methodologies developed by Isella and Manca, as described in [13, 14] and subsequently integrated in [15]. Constant parameters are obtained from technical reports and peer-reviewed scientific literature. Weighting factors are fine-tuned based on a combination of parametric analysis and engineering judgment, reflecting the relative importance of each objective term. Parameters such as $t_{regulation}$ and α are selected as compromises between, respectively, model accuracy and computational efficiency, and between error correction speed and reference production oscillations.

The two buffer units and the electrolyzer are assumed to be highly flexible, with no limitations related to rapid variations in ramping rates. Additionally, the self-discharge of both buffer units is considered negligible, and the charging and discharging efficiencies of the hydrogen tank are assumed to be unity, implying no hydrogen losses.

The one-year dynamic simulation required 2106 s of CPU time on a conventional Windows computer (Intel Core i7-1195G7 @ 2.9 GHz, 11th generation, 16 GB RAM), running Python code pre-compiled using Numba JIT. The average computation time per simulation step was 0.24 s, demonstrating that the proposed methodology is compatible with real-time execution.

The results of the case study show that the average renewable and grid power supplied to the battery energy storage system (BESS) and the electrolyzer is approximately 54.16 MW. This value is consistent with the electrolyzer energy demand under nominal operating conditions, as expressed by:

$$E_{el}^{nominal} = F_{plant}^{nominal}/c_{el} \approx 54\,MW \quad (23)$$

where $F_{plant}^{nominal} = 1000\frac{kg_{H_2}}{h}$ and $c_{el} = 18.5\ kg_{H_2}/MWh$.

Both the BESS and the hydrogen tank exhibit similar seasonal trends, with higher state-of-charge levels during the summer and nearly depleted conditions during the winter. The BESS, however, experiences larger fluctuations due to its smaller capacity. The sizing methodology [15] results in a BESS capacity of 31.81 MWh and a tank capacity of 14.58 t_{H_2}. Consequently, the BESS frequently reaches full charge or discharge to mitigate renewable power variability.

As expected, the electrolyzer operates predominantly near its nominal capacity to ensure the target hydrogen production rate of 1000 kg_{H_2}/h. Owing to its high flexibility, the electrolyzer exhibits frequent load variations, which contribute to a reduced required BESS capacity relative to the hydrogen tank. The larger tank size is also justified by the stringent constraints imposed by the downstream plant, which require the hydrogen flow rate to remain within the range of 700 to 1100 kg_{H_2}/h, as can be seen in **Figure 3**. In this context, the tank plays a crucial role in ensuring operational stability and preventing sudden and large fluctuations in hydrogen supply.

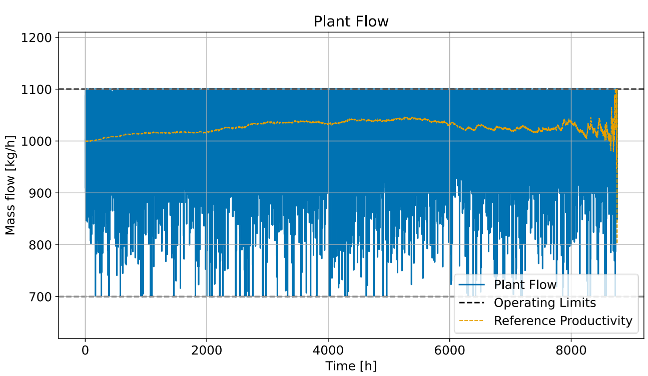

Figure 3: Hydrogen flow rate to the downstream plant.

A comparison between the hydrogen flow rate obtained in this scenario and that of a configuration without scheduling and buffer systems highlights the importance of the proposed approach. In the absence of buffers and scheduling, operational constraints are systematically violated, and the plant fails to meet its required operating limits.

From an economic standpoint, the minimum levelized cost of hydrogen (LCOH), accounting only for capital expenditure, is given by:

$$LCOH_{min} = \frac{CAPEX}{M_{H2}^{total}} = \frac{\sum_j size_j \cdot \frac{cost_j}{life_j}}{M_{H2}^{total}} = 3.00\frac{USD}{kg_{H_2}} \quad (24)$$

where the capital cost is defined as the sum of the purchase costs of each unit divided by their respective expected lifetimes.

The actual LCOH also includes the cost of electricity consumption and the effective hydrogen production. In the present analysis, revenues from selling excess electricity to the grid are not considered, and the excess renewable generation is curtailed; therefore, the resulting LCOH represents a conservative estimate. Assuming a constant electricity price of 100 USD/MWh, the final LCOH is:

$$LCOH_{eff} = \frac{CAPEX + cost_{grid} \cdot E_{grid}^{buy}}{M_{H2}^{\theta_{tot}}} = 3.31\frac{USD}{kg_{H_2}} \quad (25)$$

The total hydrogen production over the simulation period amounts to 8759.949 t_{H_2}, compared to a target value of 8760 t_{H_2}. The discrepancy of 51 kg_{H_2} is considered negligible and can be attributed to forecast–reality mismatches. First, industrial flowmeters typically exhibit an accuracy of approximately 0.25%, corresponding to a minimum detectable deviation of about 22 t_{H_2}, which is several orders of magnitude larger than the observed difference. Second, contractual agreements with the downstream plant are assumed to allow for limited operational flexibility, such that a deviation of 0.0006% does not incur penalties. Finally, at the end of the simulation, approximately 670 kg_{H_2} of hydrogen remains available in the tank, allowing the missing production to be compensated without violating any operational constraints and fully compensating for the observed overproduction.

From an environmental perspective, the only emissions associated with hydrogen production in the proposed system originate from grid electricity generation. The simulation indicates a grid electricity consumption of 26.94 GWh, which corresponds to estimated emissions of 0.92 kg_{CO_2}/kg_{H_2}, assuming a grid emission factor of 0.3 kg_{CO_2}/kWh.

This emission intensity can be compared with conventional hydrogen production pathways, such as steam methane reforming and water-gas shift processes, whose emissions are typically estimated to range from 10 kg_{CO_2}/kg_{H_2} for natural gas-based systems to 26 kg_{CO_2}/kg_{H_2} for coal-based systems. The proposed approach therefore achieves a reduction of more than one order of magnitude relative to conventional technologies.

The current system configuration does not explicitly include the compression stage between the electrolyzer, the hydrogen tank, and the downstream plant. However, a post-processing analysis indicates that incorporating the compression system would increase the final LCOH by less than 3%.

The specific compression work is evaluated based on the inlet and outlet pressures (corresponding to the electrolyzer outlet pressure and the tank inlet pressure, representing the case with the largest pressure differential), the electrolyzer operating temperature, the compressor efficiency, and the thermodynamic properties of hydrogen:

$$l_{spec}^{comp} = \frac{1}{\eta_{comp}} \cdot \frac{\gamma}{\gamma - 1} \cdot \frac{R}{MW_{H_2}} \cdot T_1 \cdot \left[\left(\frac{P_2}{P_1} \right)^{\frac{\gamma - 1}{\gamma}} - 1 \right] \qquad (26)$$

Assuming a pressure ratio of 30, an inlet temperature of 60 °C, and a compressor efficiency of 0.6, the resulting specific compression work is 0.004 MWh/kg_{H_2}.

If the required compression energy is supplied exclusively from the grid and only in the absence of renewable energy surplus, the updated LCOH becomes 3.42 USD/kg_{H_2}. This corresponds to an increase of less than 3%, or 0.11 USD/kg_{H_2}, relative to the configuration without the compression unit.

CONCLUSIONS

This work presents a novel approach for the scheduling of hydrogen production plants. The proposed framework introduces a robust methodology that solves a multidimensional optimization problem over a receding horizon, enabling the delivery of a target hydrogen flow rate to the downstream plant while simultaneously reducing unit stress and grid electricity consumption, and ensuring strict compliance with all operational constraints.

The use of imperfect renewable energy forecasts significantly enhances the realism of the analysis and demonstrates the robustness of the methodology in managing discrepancies between forecasted and actual energy availability. Despite these mismatches, the system consistently satisfies all operational constraints. A further key feature of the proposed approach is its ability to guarantee the target hydrogen productivity through dynamic adjustment of the operating reference production.

From an economic standpoint, the resulting levelized cost of hydrogen (LCOH) is consistent with values reported in the literature and remains below current industrial hydrogen production costs. From an environmental perspective, the methodology achieves a reduction in carbon dioxide emissions of approximately one order of magnitude compared to conventional hydrogen production pathways, such as natural gas- or coal-based processes.

The proposed approach is fully automated and does not require human intervention during operation, thereby reducing the risk of human-related errors. The operator's role is limited to system supervision and fault detection. Furthermore, the methodology is general in nature and can be readily adapted to existing industrial facilities, offering a practical pathway to improve operational efficiency and overall system performance.

Despite these advantages, several limitations should be acknowledged. First, the renewable energy forecast model lacks full accuracy, as it is derived as a post-processing step from real energy profiles. Additionally, the stochastic component is defined as a fixed percentage of the filtered profile, resulting in increasing absolute deviations at higher renewable generation levels (e.g., during summer periods), even though the relative error remains constant. Second, operational and maintenance costs are not included in the LCOH calculation, which would lead to a higher overall cost estimate. Third, the electricity price is assumed to be constant, whereas in practice it is time-dependent and subject to market variability. Finally, although its contribution is relatively minor, the compression system should be explicitly integrated into the main system model.

Future developments may include the extension of the methodology to islanded systems, where access to grid electricity is not available. In addition, a more detailed and explicit modeling of downstream processes, such as ammonia or methanol synthesis plants, would further enhance the industrial relevance and applicability of the proposed approach.

AUTHOR IDENTIFIERS

Author ORCIDs:
Lea Casagrande M: 0009-0009-5672-3041
Isella A: 0000-0002-3699-4698
Manca D: 0000-0003-2055-9752

REFERENCES

1. IEA. Global Energy Review 2025 (2025). https://www.iea.org/
2. WRI. Where Do Emissions Come From? 4 Charts Explain Greenhouse Gas Emissions by Sector (2024). https://www.wri.org/insights/4-charts-explain-greenhouse-gas-emissions-countries-and-sectors
3. Eurostat. Renewable Energy Statistics (2024). https://ec.europa.eu/eurostat/statisticsexplained/
4. Hasan MM, Genç G. Techno-economic analysis of solar/wind power based hydrogen production. Fuel 324:124564 (2022). https://doi.org/10.1016/j.fuel.2022.124564
5. Isella A, Ostuni R, Manca D. Towards the decarbonization of ammonia synthesis – a techno-economic assessment of hybrid-green process alternatives. Chemical Engineering Journal 486:150132 (2024).

https://doi.org/10.1016/j.cej.2024.150132
6. Roy TK. Techno-economic and environmental assessment of green hydrogen production in multiple australian regions using different electrolyzer technologies. Renewable Energy 256:123879 (2026). https://doi.org/10.1016/j.renene.2025.123879
7. Salmon N, Bañares-Alcántara R. Impact of process flexibility and imperfect forecasting on the operation and design of haber–bosch green ammonia. RSC Sustainability 1:923-937 (2023). https://doi.org/10.1039/d3su00067b
8. Schmitt T, Engel J, Kopp M, Rodemann T. Implicit incorporation of heuristics in mpc-based control of a hydrogen plant. 2023 IEEE International Conference on Power Electronics, Smart Grid, and Renewable Energy (PESGRE) :1-8 (2023). https://doi.org/10.1109/pesgre58662.2023.10404171
9. García CE, Prett DM, Morari M. Model predictive control: theory and practice—a survey. Automatica 25:335-348 (1989). https://doi.org/10.1016/0005-1098(89)90002-2
10. Morari M, H Lee J. Model predictive control: past, present and future. Computers & Chemical Engineering 23:667-682 (1999). https://doi.org/10.1016/s0098-1354(98)00301-9
11. Marcucci T, Tedrake R. Warm start of mixed-integer programs for model predictive control of hybrid systems. IEEE Trans. Automat. Contr. 66:2433-2448 (2021). https://doi.org/10.1109/tac.2020.3007688
12. CAISO. Production and curtailments data (2025). https://www.caiso.com/library/production-curtailments-data
13. Isella A, Manca D. A framework for the design of battery energy storage systems in power-to-x processes. Journal of Energy Storage 123:116744 (2025). https://doi.org/10.1016/j.est.2025.116744
14. Isella A, Manca D. A general criterion for the design and operation of flexible hydrogen storage in power-to-x processes. International Journal of Hydrogen Energy 99:649-660 (2025). https://doi.org/10.1016/j.ijhydene.2024.12.228
15. Isella A, Manca D. Integrating economic, environmental, and social sustainability in power-to-ammonia plants: a multi-objective optimization methodology. Computers & Chemical Engineering 198:109082 (2025). https://doi.org/10.1016/j.compchemeng.2025.109082